

Supporting information

## Interfacial Engineering of Vertically-stacked Graphene/h-BN Heterostructure as an Efficient Electrocatalyst for Hydrogen Peroxide Synthesis

Yuying Zhao<sup>a,b,#</sup>, Xiang Xu<sup>a,#</sup>, Qixin Yuan<sup>a</sup>, Yuhan Wu<sup>a</sup>, Kang Sun<sup>b</sup>, Bei Li<sup>b</sup>, Zeming Wang<sup>c</sup>, Ao Wang<sup>b</sup>, Hao Sun<sup>b</sup>, Mengmeng Fan<sup>a,b,\*</sup>, Jianchun, Jiang<sup>a,b</sup>

<sup>a</sup> Jiangsu Co-Innovation Center of Efficient Processing and Utilization of Forest Resources, International Innovation Center for Forest Chemicals and Materials, College of Chemical Engineering, Nanjing Forestry University, Nanjing, 210037, China  
E-mail: fanmengmeng370@njfu.edu.cn

<sup>b</sup> Key Lab of Biomass Energy and Material, Jiangsu Province; Jiangsu Co-Innovation Center of Efficient Processing and Utilization of Forest Resources, Institute of Chemical Industry of Forest Products, Chinese Academy of Forestry, Nanjing, 210042, China

<sup>c</sup> Institute of Nanochemistry and Nanobiology, School of Environmental and Chemical Engineering, Shanghai University, Shanghai, 200444, China

# These two authors contributed equally to this work.

### Experimental section

#### Synthesing C-BN, porous h-BN and N-C

Boric acid (0.618 g), dicyandiamide (2.7 g), 1, 3, 6 - trinitropyrene (50 mg) were dispersed into 50 ml deionized water in a 200 ml beaker and then above solution was sonicated for 1 h (200 W). The solution was fiercely stirred and heated on a hot plate until all water completely evaporated. The obtained solid was ground into powders in a mortar and then calcined at 800 °C for 3 h under NH<sub>3</sub> (50 sccm) in a resistance-heating horizontal furnace. After cooling to room temperature, we can get porous C-BN samples. In order to control the C content, various 1, 3, 6 – trinitropyrene amounts (20, 100 or 200 mg) were added and the corresponding samples were defined as C-BN-20, -100 and -200, respectively. The porous h-BN was prepared by the same progress except no addition of trinitropyrene. The N-C was prepared by directly annealing trinitropyrene at 800 °C for 3 h under NH<sub>3</sub> (50 sccm). The commercial h-BN powders were purchased from Sigma-Aldrich. The 1, 3, 6 – trinitropyrene was prepared according to the previous research<sup>14</sup>.

#### Liquid N<sub>2</sub> assisted Exfoliation

The sample (C-BN, BN and commercial h-BN) was placed in liquid N<sub>2</sub> for 20 min and then the solution (isopropanol: DI (V/V) =1:1) was quickly added with the concentration of 1 mg ml<sup>-115</sup>. The mixing solution was continuously sonicated for 10 h (200 W). The exfoliated nanosheets are separated by centrifugation (3000 rpm, 5min). The supernatant is used for the application of catalyst ink.

#### Model experiments

The GQDs was prepared according to the previous research<sup>14</sup>. The 40 μl GQDs in isopropanol (2.5 mg ml<sup>-1</sup>) and 200 μl supernatant of exfoliated commercial h-BN was mixed and diluted to 1 ml with isopropanol. After overnight magnetic stirring, 5 wt% Nafion solution (50 μl) and carbon black (2 mg) were added into the solution. After the sonication (200 W, 2 h), the G/h-BN catalyst ink was prepared. The other measuring conditions are same to those of C-BN.

#### Electrochemical characterization

All the electrochemical tests were carried out in an electrochemical workstation (Chenhua CHI760E) with a three-electrode system. A RRDE electrode with a disk glassy carbon electrode area of 0.2475 cm<sup>2</sup> and Pt ring area of 0.1866 cm<sup>2</sup> was used as the working electrode. A graphite rod and a Hg/HgO electrode acted as the counter electrode and reference electrode, respectively. The supernatant (1 ml) after the liquid N<sub>2</sub>-assisted exfoliation was mixed with carbon black (2 mg) and 5wt% Nafion solution (50 μl) by sonication (200 W, 2h) as the catalyst ink. 10 μl ink was dopped onto RRDE electrode and dried at room temperature. Linear sweep voltammetry (LSV) curves were conducted in O<sub>2</sub> saturated 0.1 M KOH solution at a scan rate of 10 mV s<sup>-1</sup> at the speed of 1600 rpm. The solution resistance (R<sub>s</sub>) was not compensated. A potential of 1.2 V vs. RHE was applied at the ring electrode. The H<sub>2</sub>O<sub>2</sub> selectivity and electron transfer number were calculated by the following equations based on the LSV curves.

$$\text{H}_2\text{O}_2 \text{ yield (\%)} = 200 \times \frac{I_R/N}{I_D + I_R/N} \quad (1)$$

$$N = \frac{4|I_D|}{I_D + I_{R/N}} \quad (2)$$

Where  $I_R$  is the ring current,  $I_D$  is the disk current, and  $N$  is the collection efficiency (0.37 after calibration).

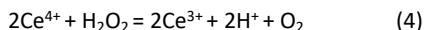
**Electrochemical measurement in a flow cell:** A flow cell setup is a two-compartment cell with a cation exchange membrane as a separator. 150  $\mu$ l C-BN catalyst ink (1 ml supernatant with 4 mg carbon black) was deposited on the gas diffusion layer electrode (GDL, HESEN HCP120) (working area 1 cm<sup>2</sup>) with a loading of 0.6 mg cm<sup>-2</sup> (the amount of carbon black) as the cathode. The Pt film and Ag/AgCl electrode were used as the anode and reference electrodes, respectively. In the two compartments, 0.1 M KOH (300 mL) was used as the electrolyte and was recycled through each compartment at the flow rate of 20 ml min<sup>-1</sup>. O<sub>2</sub> was fed at the rate of 40 ml min<sup>-1</sup> to the cathode. The electrosynthesis of H<sub>2</sub>O<sub>2</sub> was performed at a fixed potential 0.2 V vs. RHE.

The faradaic efficiency (FE) of H<sub>2</sub>O<sub>2</sub> was calculated according to the following equation:

$$FE (\%) = \frac{2CVF}{Q} * 100\% \quad (3)$$

where  $C$  represents the concentration of H<sub>2</sub>O<sub>2</sub> (mol l<sup>-1</sup>) in the electrolyte,  $V$  the volume of electrolyte (l),  $F$  Faraday constant (96485 C mol<sup>-1</sup>),  $Q$  total charge amount (C) during the reaction. The  $Q$  was determined by integral operation in the electrochemical workstation:

The H<sub>2</sub>O<sub>2</sub> concentration in the electrolyte was measured by a titration method using Ce(SO<sub>4</sub>)<sub>2</sub>. The adding of H<sub>2</sub>O<sub>2</sub> leads to the conversion from yellow Ce<sup>4+</sup> to colorless Ce<sup>3+</sup> in the following reaction:



According to the equation, the  $C_{H_2O_2}$  was calculated based on the equation:

$$C_{H_2O_2} = 1/2 \Delta C_{Ce^{4+}} \quad (5)$$

UV-V is spectroscopy was used to make the linear calibration curve between Ce<sup>4+</sup> concentration and the Ce<sup>4+</sup> absorbance at 317 nm.

### Characterization

The morphology was characterized by high-resolution TEM (FEI Talos F200s) with Energy dispersive X-ray element detector (FEI Super-X EDS Detector). The structure and composition were characterized by X-ray photoelectron spectra (Thermo Scientific Al K<sub>α</sub>), X-ray diffractometer (Bruker, D8 FOCUS) equipped with a Cu K<sub>α</sub> radiation source ( $\lambda=0.154$  nm), FT-IR (Nicolet IS10). The Raman spectra were measured by a Renishaw inVia with a 532 nm laser source. The surface area and meso/macropore size distributions of the as-prepared materials were determined by the Brunauer-Emmett-Teller (BET) and Barret-Joyner-Halenda (BJH) methods, respectively. N<sub>2</sub> adsorption-desorption isotherm tests were performed on a gas adsorption analyzer (ASAP2460, Micromeritics).

### DFT simulation

We used the Vienna Ab-initio Simulation Package (VASP, 5.4.4) code54, 55 with GGA-PBE exchange-correlation functional56 for DFT calculations<sup>16, 17</sup>. The project-augmented wave (PAW) pseudopotential57, 58 for describing the core-valence interactions and cutoff of 450 eV were used<sup>18</sup>. h-BN and graphene were known to have very similar lattice constant ( $a_{h-BN} = 2.504$  Å<sup>19</sup> and  $a_{Graphene} = 2.464$  Å<sup>20</sup>). In this study, we performed two monomer calculations using graphene's in-plane lattice parameters to directly compare the screening effects of each material. Furthermore, we assumed a thickness of ~20 Å for the vacuum layer to prevent the interaction between periodic images. In addition, we considered three different stacked configurations (AA' stacking, B-centered AB stacking, and N-centered AB stacking) for the monolayer h-BN/Graphene interface. The Brillouin zone in reciprocal space was sampled using Monkhorst-Pack scheme59, and the geometric/electronic structure optimization was performed using 1×1×1 and 2×2×1 k point meshes<sup>21, 22</sup>.

The Gibbs free energy of the 2 e<sup>-</sup> ORR elementary steps is calculated using the computational hydrogen electrode (CHE) model, defined as  $\Delta G_n(U) = \Delta G_n(U=0) + neU$ , where  $n$  is the number of e<sup>-</sup> transferred in reaction and  $U$  is the potential of the electrode to the reversible hydrogen electrode (RHE)<sup>23</sup>. At  $U=0V$ ,  $\Delta G_n = \Delta E_n - \Delta S + \Delta ZPE$ , where  $\Delta E_n$  is DFT-calculated reaction energy in vacuum,  $T\Delta S$  is the entropy contributions to reaction at  $T = 298.15$  K,  $\Delta ZPE$  is zero-point energy (ZPE) correction based on the calculated vibrational frequencies. The free energy of O<sub>2</sub>(g) was derived as  $G_{O_2(g)} = 2G_{H_2O(l)} - 2G_{H_2} - 4 \times 1.23$  eV since the high-spin ground state of an oxygen molecule is notoriously poorly described in DFT calculations.

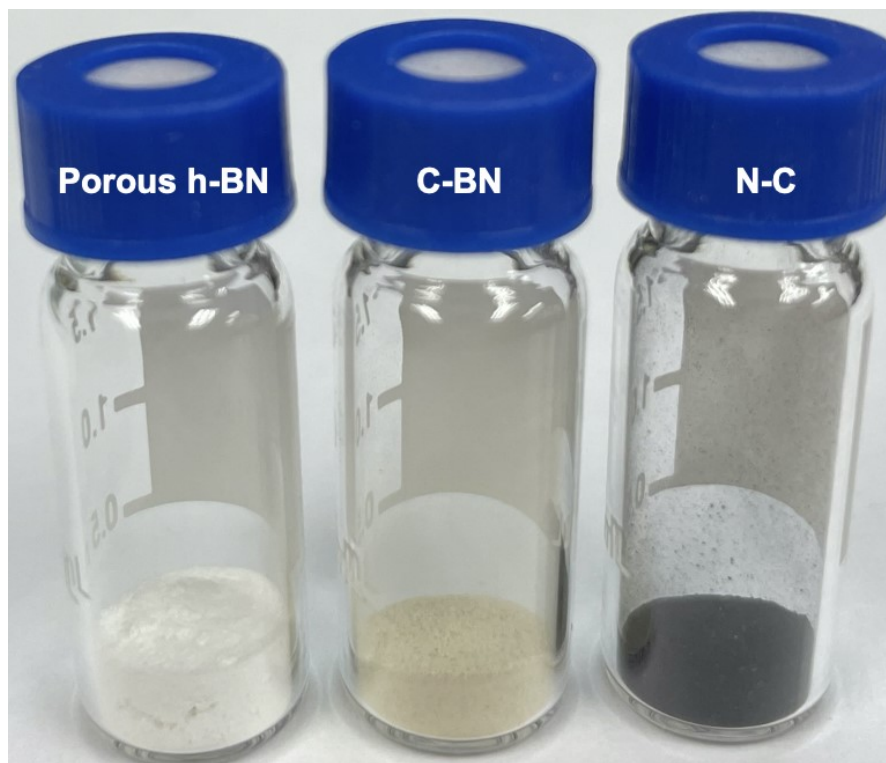


**Fig. S1.** The photograph of different samples

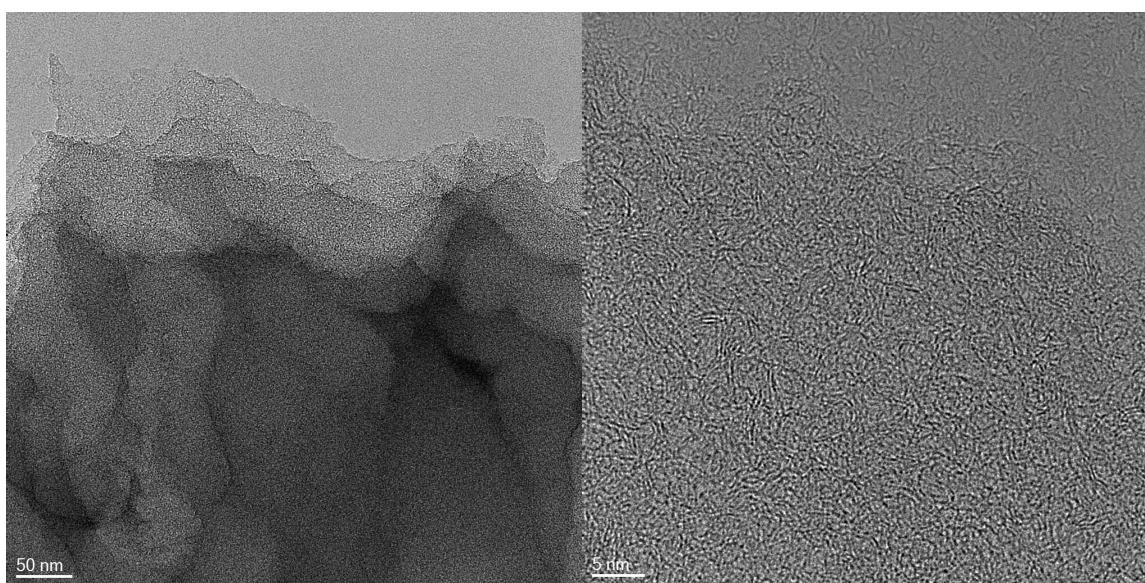


**Fig. S2.** The HR-TEM image of N-C.

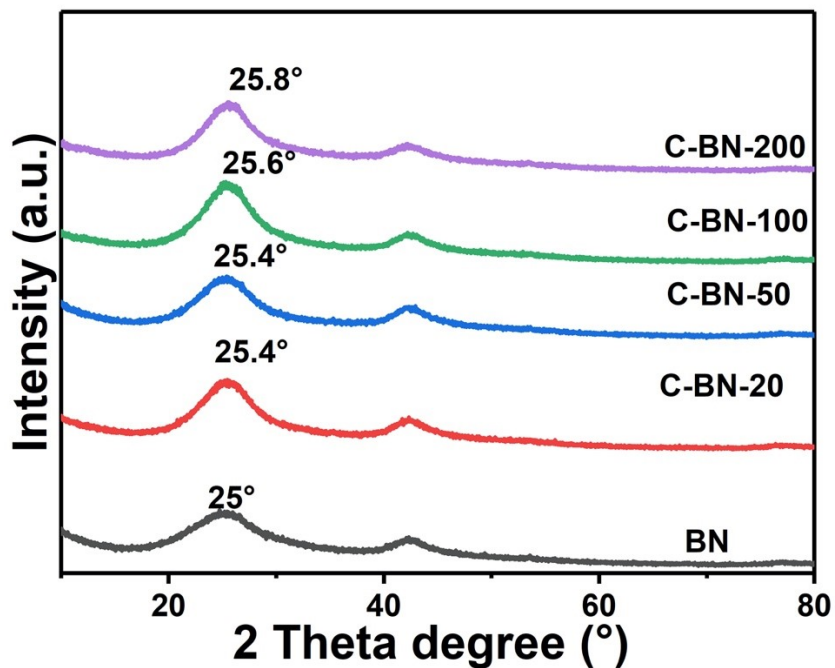


Fig. S3. The XRD patterns for C-BN-x samples

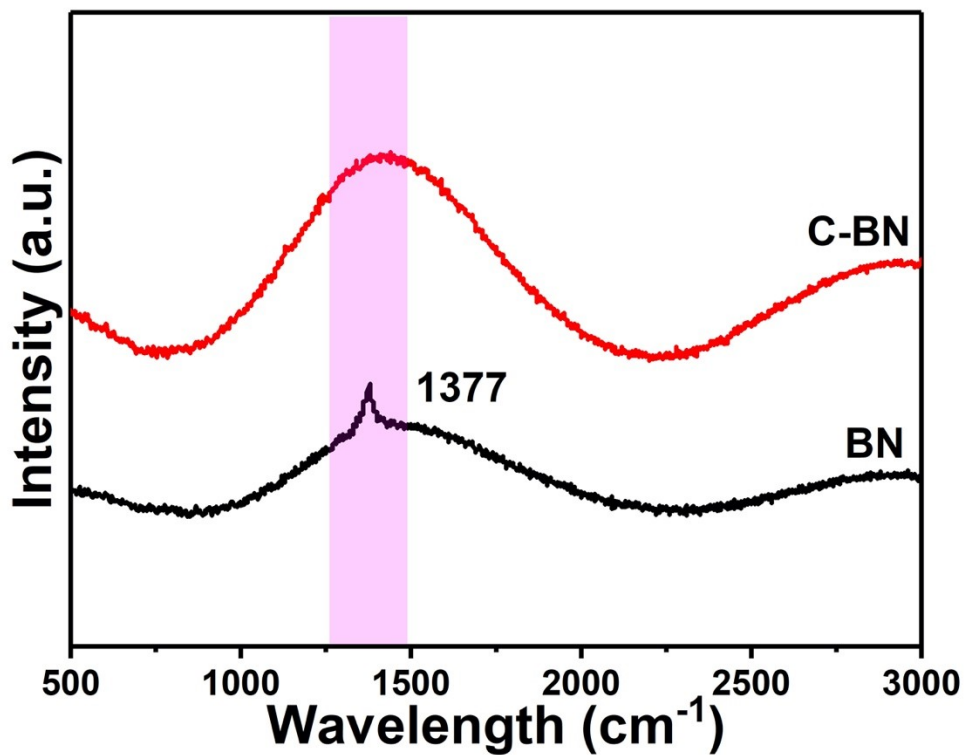


Fig. S4. The Raman spectrum of C-BN and BN

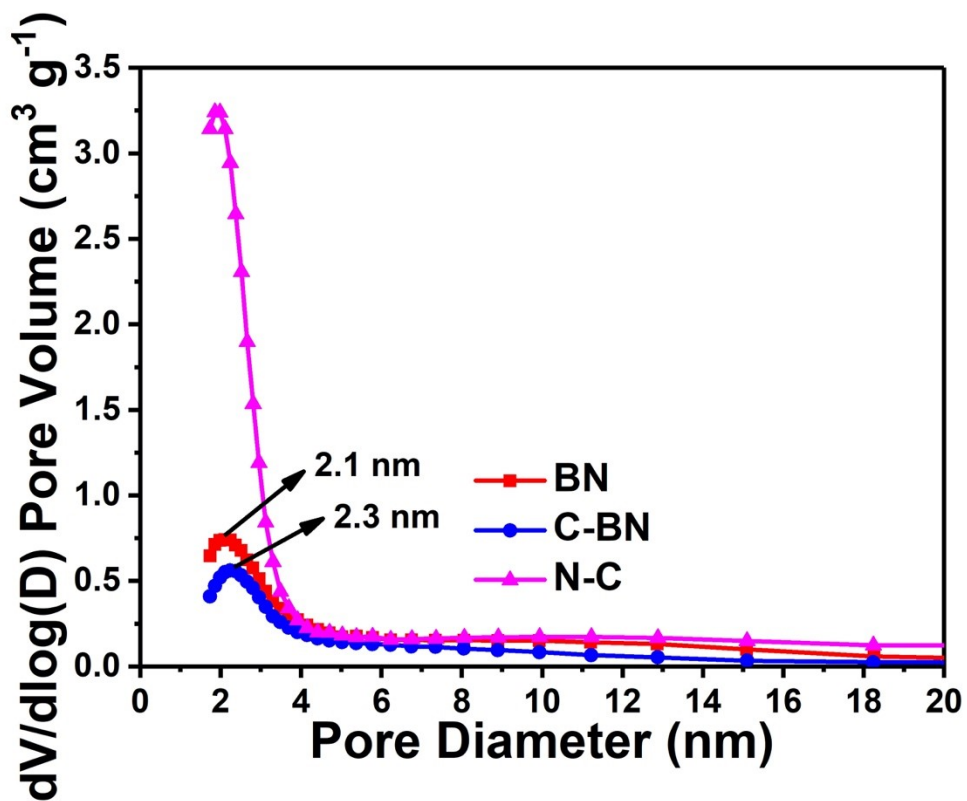


Fig. S5. The pore diameter distribution of BN, N-C and C-BN

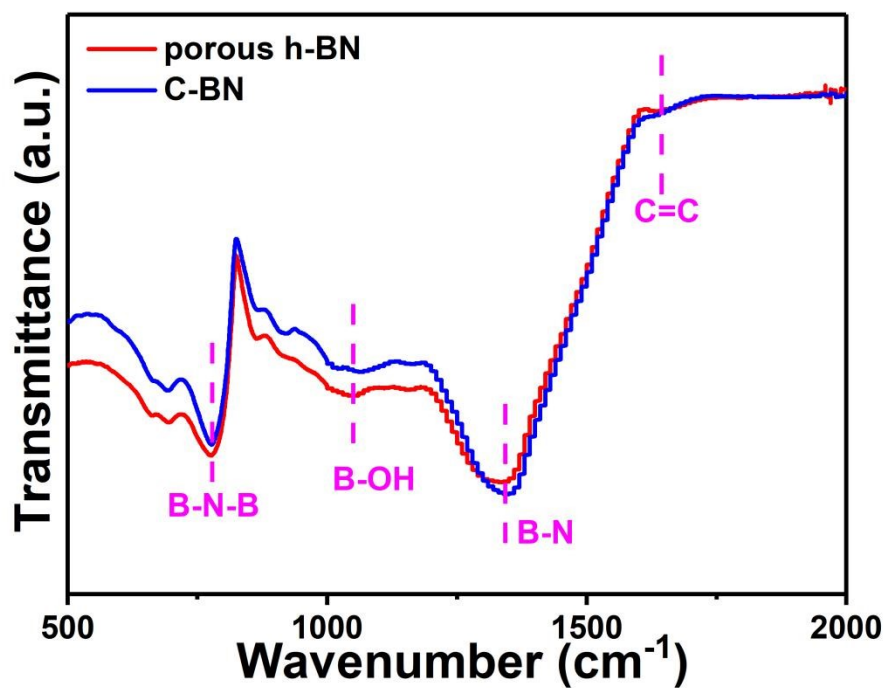


Fig. S6 The FT-IR spectrum for C-BN and porous h-BN.

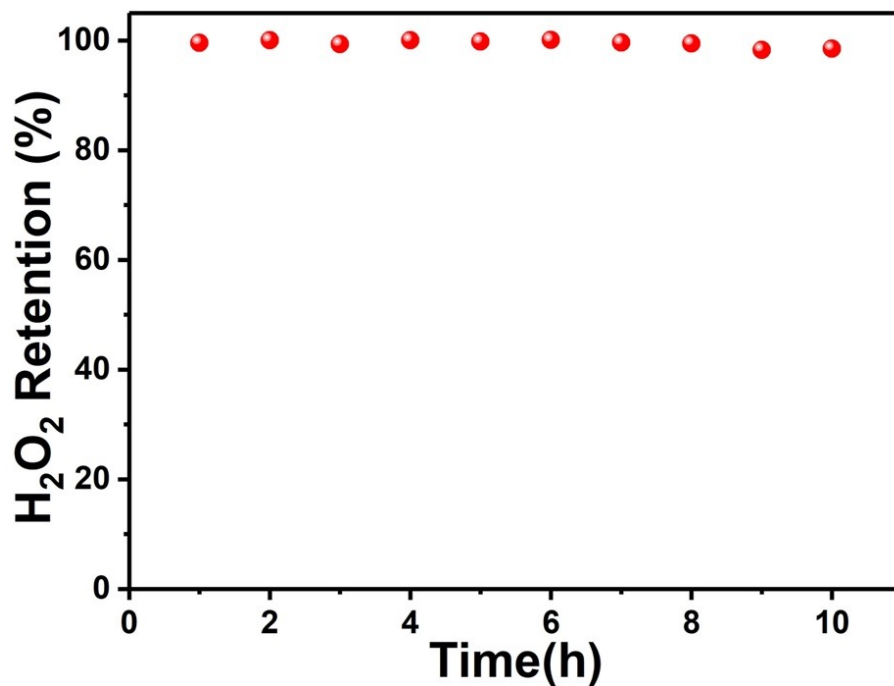


Fig. S7. The retention rate of 26 mM H<sub>2</sub>O<sub>2</sub> in 0.1 M KOH solution during 10 h at room temperature and out of light.

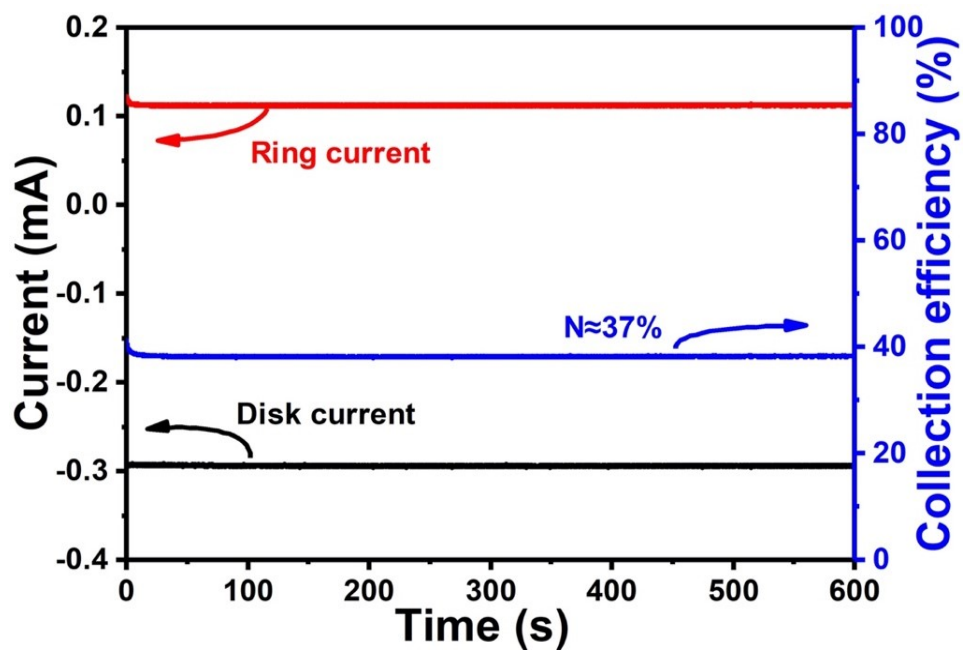


Fig. S8 The RRDE at 1600rpm measured in 2 mM K<sub>3</sub>[Fe(CN)<sub>6</sub>] in 0.1M KOH solution

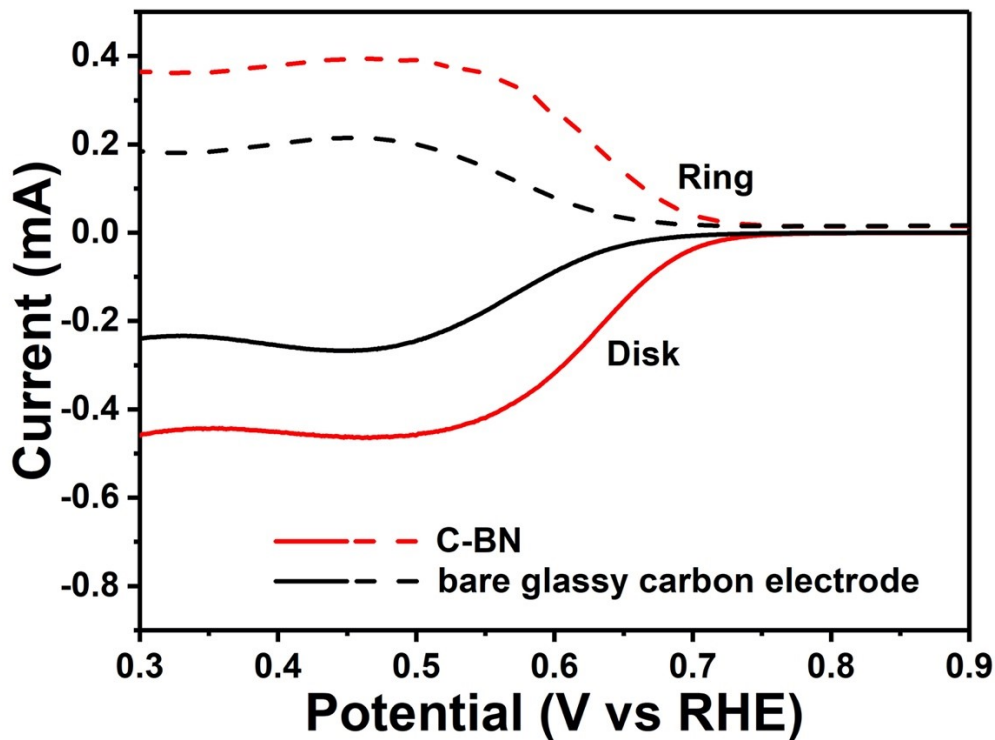


Fig. S9 The LSV curves of C-BN and bare GCE of RRDE in  $O_2$ -saturated 0.1 M KOH solution at 1600 rpm.

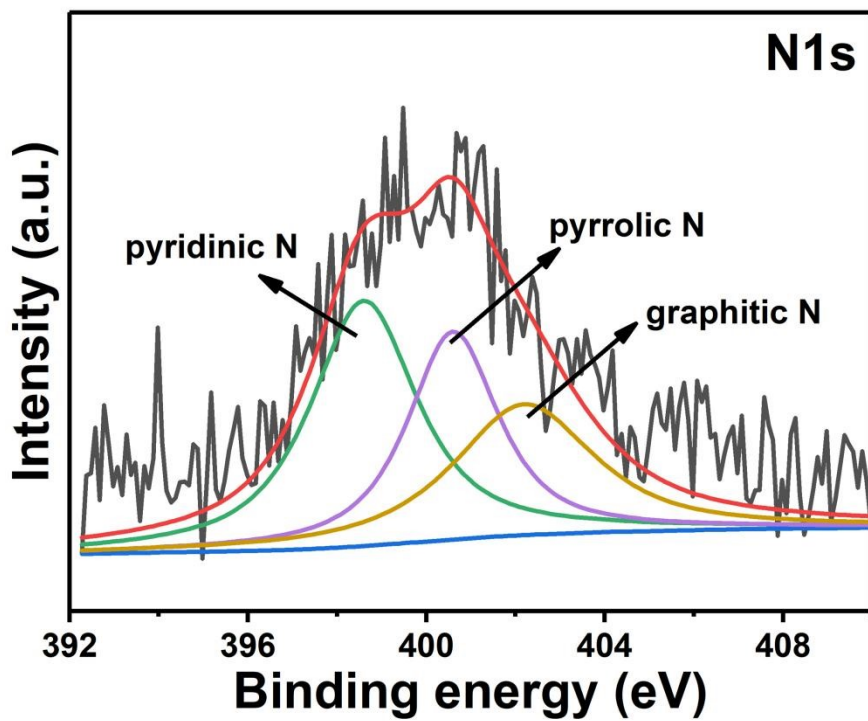


Fig. S10 The N1s spectrum of N-C.

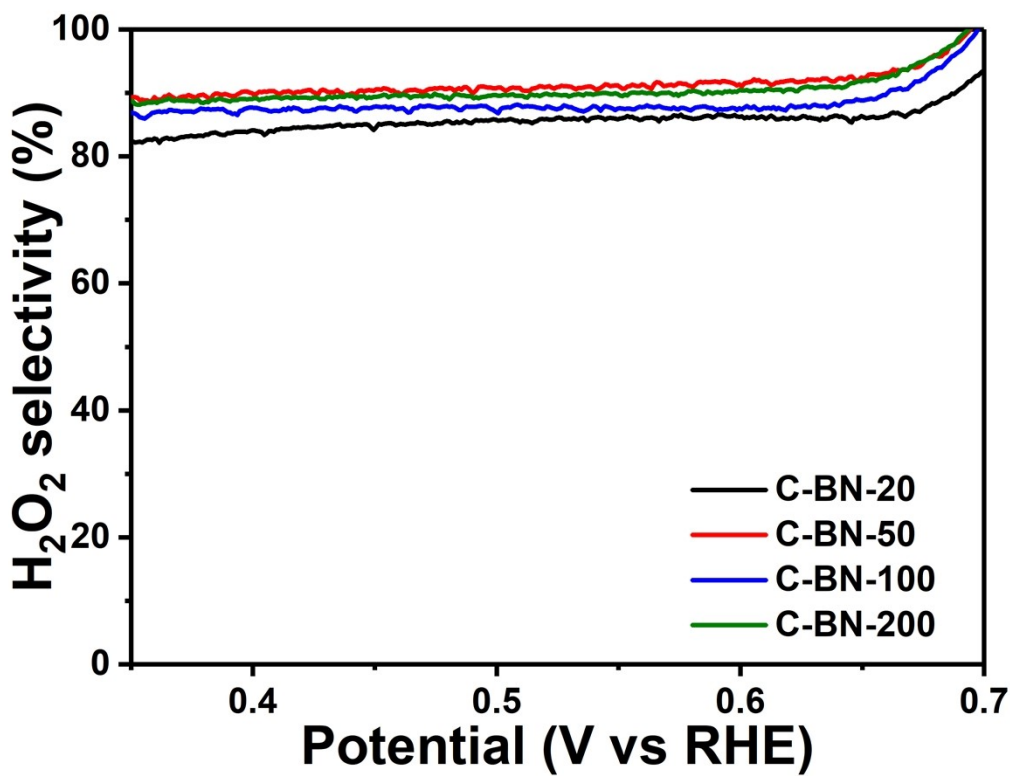
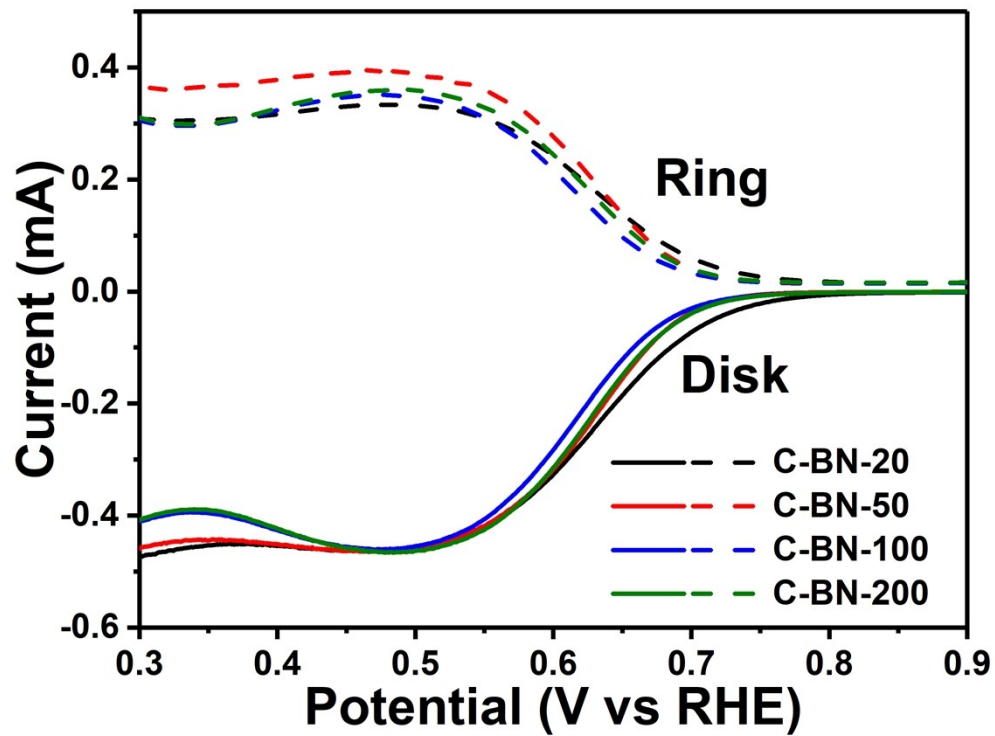


Fig. S11 The LSV curves and H<sub>2</sub>O<sub>2</sub> selectivity of C-BN-x

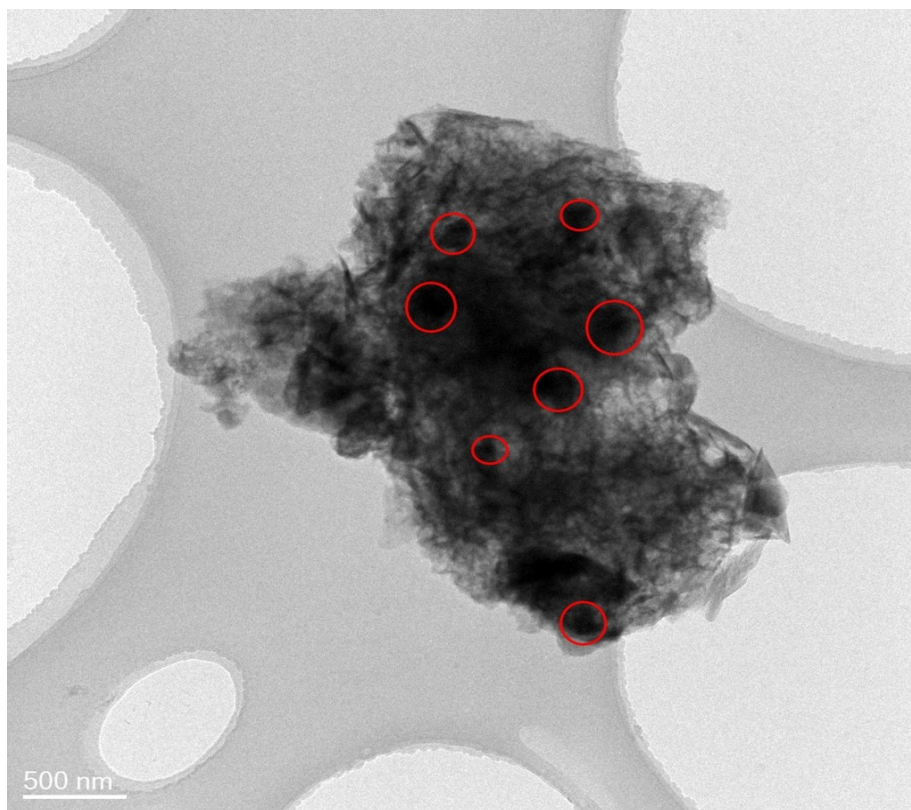


Fig. S12 The HR-TEM image of C-BN-200 (carbon nanosheets remarked with red circles)

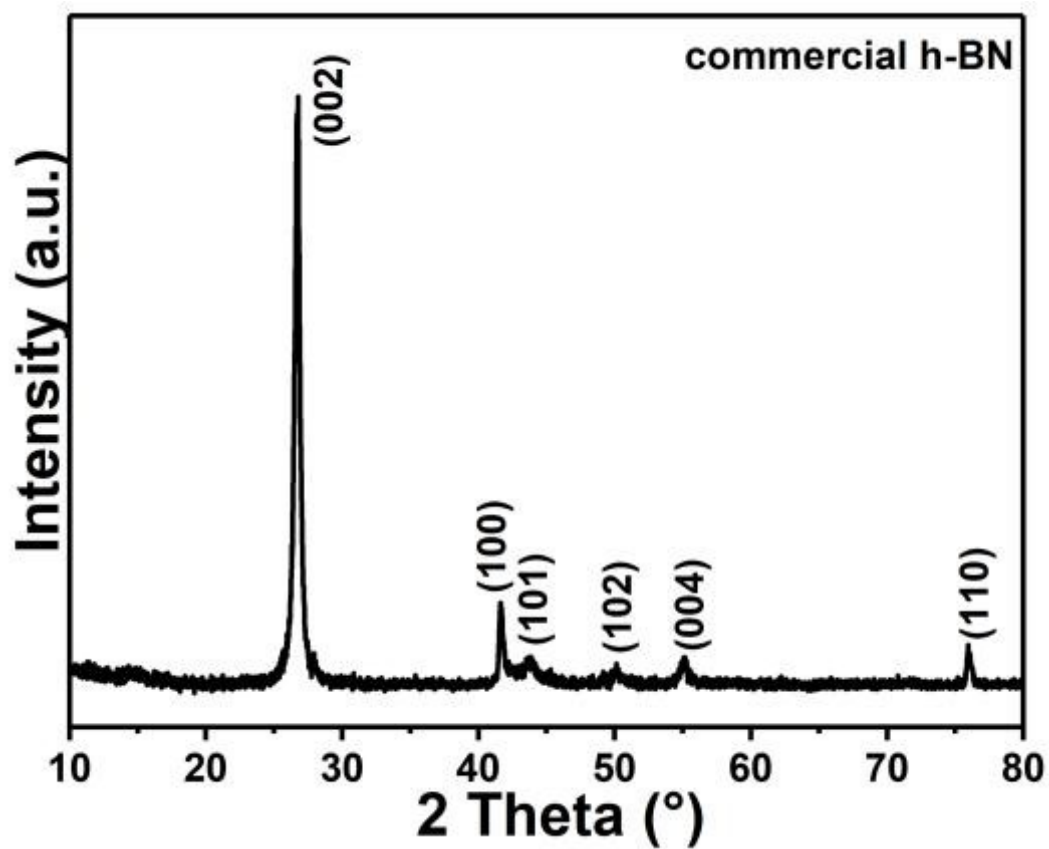


Fig. S13 The XRD pattern of commercial h-BN with high crystal structure

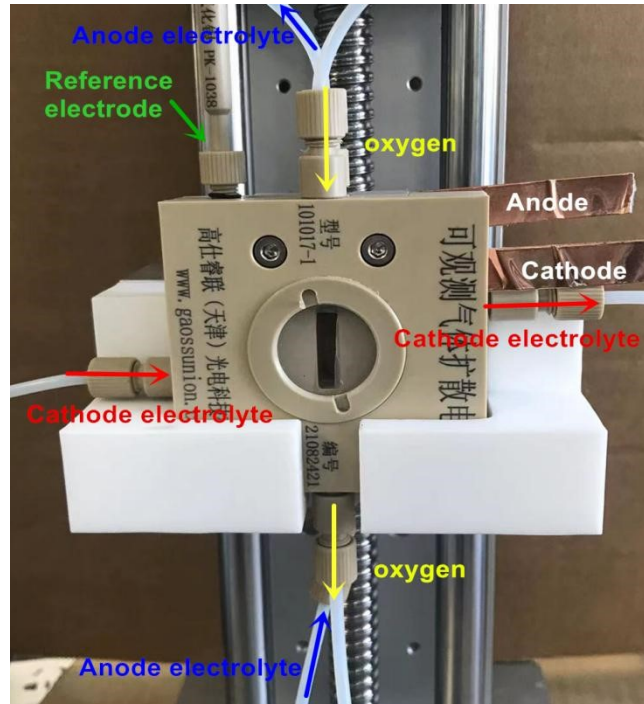


Fig. S14 The image of the actual flow cell setup.

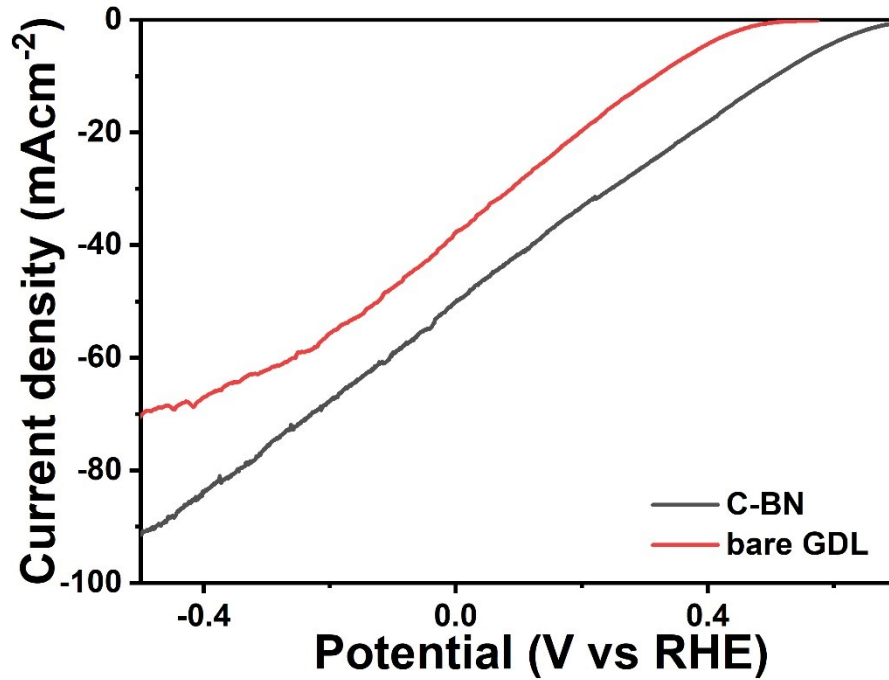


Fig. S15 The LSV curves of flow cell setup with the C-BN as the catalyst in GDL electrode and the bare GDL electrode at the scan rate of 10 mV s<sup>-1</sup>.

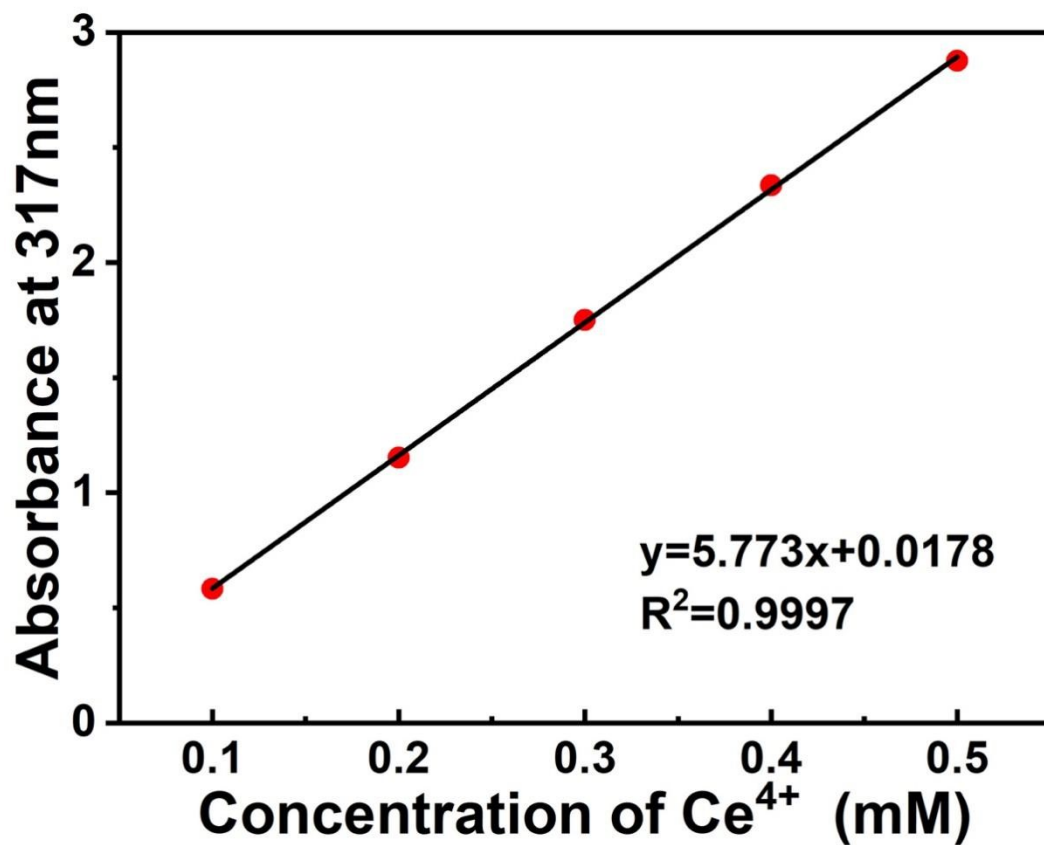


Fig. S16 The linear calibration curve between the Ce<sup>4+</sup> concentration and absorbance at 317 nm.

**Table S1.** The C contents for various samples measured by elemental analyzer.

Samples	Porous h-BN	C-BN-20	C-BN-50	C-BN-100	C-BN-200
wt.%	/	/	0.19%	0.42%	4.20%

**Table S2.** The activity summary of many reported electrocatalysts in alkaline electrolyte

<b>electrocatalyst</b>	<b>selectivity</b>	<b>Range</b>	<b>Ref.</b>
single atom Co@N-doped carbon, Co-N-C	below 80%	0.1-0.8 V	[1]
single atoms Pd on CNTs (Pd-O-C)	90%-95%	0.1-0.5 V	[2]
metallic cobalt diselenide (CoSe <sub>2</sub> )	~50%-82%	0-0.4 V	[3]
single Fe @CNTs (Fe-C-O)	~80%-92%	0.4-0.7 V	[4]
atomic Co @N-doped carbon, Co-N <sub>x</sub> -C	~75%-85%	0.5-0.8 V	[5]
single Mo @ O/S doped carbon, Mo-OS-C	~93%-97%	0.4-0.7 V	[6]
atomically Al on carbon, Al-O-C	~93-95%	0.4-0.65 V	[7]
edge rich carbon	~91-94%	0.2-0.6 V	[8]
oxidized CNTs, O-CNTs	~84%-88%	0.4-0.7 V	[9]
boron nitride doped carbon, BN-C	~72%-87%	0.2-0.7 V	[10]
B-rich borocarbonitride (BCN)	~70%	0.2-0.6 V	[11]
B, N-codoped carbon (B, N-C)	~80%-94%	0.3-0.6 V	[12]
oxygenated B-doped carbon (O-BC)	~80%-96%	0.3-0.6 V	[13]
N, O co-doped carbon (NO-C)	~80%	0.3-0.7 V	[14]
<b>C-BN</b>	<b>90%-99%</b>	<b>0.35-0.7 V</b>	<b>This work</b>

**Table S3.** Comparing the catalytic performance and H<sub>2</sub>O<sub>2</sub> production capability between the C-BN and the recently reported electrocatalysts.

Samples	H <sub>2</sub> O <sub>2</sub> production rate (mmolg <sub>catalyst</sub> <sup>-1</sup> h <sup>-1</sup> )	H <sub>2</sub> O <sub>2</sub> Yield	Ref.
<b>C-BN</b>	<b>1167 (~40 mA cm<sup>-2</sup>)</b>	<b>35 mM, 15 h (357 mg)</b>	<b>This work</b>
oxygen-doped carbon nanosheet	770 (50 mA cm <sup>-2</sup> )	57.7 mM at 11h (196 mg)	[15]
N-doped graphene	224.8	\	[16]
Oxidized carbon nanotubes	111.7 (50 mA cm <sup>-2</sup> )	57.7 mM at 0.5h (49 mg)	[9]
honeycomb carbon nanofibers	6.37mmolL <sup>-1</sup> h <sup>-1</sup>	\	[17]
carbonyl-functionalized graphitic nanophatelets	\	6.1 mM at 30 h	[18]
reduced graphene oxide	\	57 mg at 15 h	[19]
Edge-Site-Rich Carbon	\	24.4 mM at16 h	[8]
Co–N <sub>4</sub> moiety in nitrogen-doped graphene	418 (50 mA cm <sup>-2</sup> )	170.9 mM at 30 h (58.12 mg)	[20]
Single-Co atoms in N-doped carbon	4330 (500 mA cm <sup>-2</sup> )	~ 571 mg at 6 h	[1]
Co-N <sub>x</sub> -C site and oxygen functional group modified carbon	474.2 (50 mA cm <sup>-2</sup> )	61 mg at 1.5 h	[5]
oxygenated boron-doped carbon	412.8 (~3.2 mA cm <sup>-2</sup> )	\	[13]
Hierarchically Porous Carbon	395.7-110.2	222.6-62.0 mM (151.4-42.2 mg) 2.5 h	[21]

**Table S4.** DFT-calculated Gibbs adsorption free energy values (eV) and  $U_{\text{limited}}$  (V) of key intermediates involved in the ORR on surface of vertically-stacked G/h-BN.

	Doping structures	$\Delta G_{\text{OOH}^*}$	Energy barrier (eV)	$U_{\text{limited}}$ (V)
B-centered AB stacking (model 1)	centre B	3.59	0.74	0.04
	edge B	4.15	0.06	0.64
	centre C	3.72	-0.50	0.20
	edge C	4.42	-0.56	0.41
	centre N	3.76	0.76	0.25
	edge N	4.78	0.49	0.21
N-centered AB stacking (model 2)	centre B	3.44	0.32	0.38
	edge B	4.95	0.92	-0.22
	centre C	3.13	0.62	0.08
	edge C	3.60	1.26	-0.56
	centre N	5.18	-0.12	0.58
	edge N	3.53	-1.65	-0.95
AA' stacking (model 3)	centre B	5.39	0.44	0.27
	edge B	4.90	0.36	0.34
	centre C	3.96	0.65	0.05
	edge C	5.05	-0.85	-0.15
	centre N	5.02	0.64	0.06
	edge N	5.19	-0.27	0.43

## References

- [1] Y. Sun, L. Silvioli, N. R. Sahraie, W. Ju, J. Li, A. Zitolo, S. Li, A. Bagger, L. Arnarson, X. Wang, T. Moeller, D. Bernsmeier, J. Rossmeisl, F. Jaouen, P. Strasser, *J. Am. Chem. Soc.* **2019**, *141*, 12372.
- [2] Q. Chang, P. Zhang, A. H. B. Mostaghimi, X. Zhao, S. R. Denny, J. H. Lee, H. Gao, Y. Zhang, H. L. Xin, S. Siahrostami, J. G. Chen, Z. Chen, *Nat. commun.* **2020**, *11*, 2178.
- [3] H. Sheng, E. D. Hermes, X. Yang, D. Ying, A. N. Janes, W. Li, J. R. Schmidt, S. Jin, *ACS Catal.* **2019**, *9*, 8433.
- [4] K. Jiang, S. Back, A. J. Akey, C. Xia, Y. Hu, W. Liang, D. Schaak, E. Stavitski, J. K. Nørskov, S. Siahrostami, H. Wang, *Nat. commun.* **2019**, *10*, 3997.
- [5] B.-Q. Li, C.-X. Zhao, J.-N. Liu, Q. Zhang, *Adv. Mater.* **2019**, *31*, 1808173.
- [6] C. Tang, Y. Jiao, B. Shi, J.-N. Liu, Z. Xie, X. Chen, Q. Zhang, S.-Z. Qiao, *Angew. Chem. Int. Ed.* **2020**, *59*, 9171.
- [7] Q. Yang, W. Xu, S. Gong, G. Zheng, Z. Tian, Y. Wen, L. Peng, L. Zhang, Z. Lu, L. Chen, *Nat. commun.* **2020**, *11*, 5478.
- [8] Y. J. Sa, J. H. Kim, S. H. Joo, *Angewandte Chemie International Edition* **2019**, *58*, 1100.
- [9] Z. Lu, G. Chen, S. Siahrostami, Z. Chen, K. Liu, J. Xie, L. Liao, T. Wu, D. Lin, Y. Liu, T. F. Jaramillo, J. K. Nørskov, Y. Cui, *Nat. Catal.* **2018**, *1*, 156.
- [10] S. Chen, Z. Chen, S. Siahrostami, D. Higgins, D. Nordlund, D. Sokaras, T. R. Kim, Y. Liu, X. Yan, E. Nilsson, R. Sinclair, J. K. Nørskov, T. F. Jaramillo, Z. Bao, *J. Am. Chem. Soc.* **2018**, *140*, 7851.
- [11] Z. Liu, D. Gao, L. Hu, F. Liu, H. Liu, Y. Li, J. Zhang, Y. Xue, C. Tang, *ChemistrySelect* **2022**, *7*.
- [12] X. Li, X. Wang, G. Xiao, Y. Zhu, *J Colloid Inter. Sci.* **2021**, *602*, 799.
- [13] Y. Chang, J. Li, J. Ma, Y. Liu, R. Xing, Y. Wang, G. Zhang, *Sci. China Mater.* **2022**, *65*, 1276.
- [14] H. Shao, Q. Zhuang, H. Gao, Y. Wang, L. Ji, X. Wang, T. Zhang, L. Duan, J. Bai, Z. Niu, J. Liu, *Inorg. Chemi. Front.* **2021**, *8*, 173.
- [15] S. Chen, T. Luo, K. Chen, Y. Lin, J. Fu, K. Liu, C. Cai, Q. Wang, H. Li, X. Li, J. Hu, H. Li, M. Zhu, M. Liu, *Angew. Chem. Int. Ed.* **2021**, *60*, 16607.
- [16] L. Han, Y. Sun, S. Li, C. Cheng, C. E. Halbig, P. Feicht, J. L. Hübner, P. Strasser, S. Eigler, *ACS Catal.* **2019**, *9*, 1283.
- [17] K. Dong, J. Liang, Y. Wang, Z. Xu, Q. Liu, Y. Luo, T. Li, L. Li, X. Shi, A. M. Asiri, Q. Li, D. Ma, X. Sun, *Angew. Chem. Int. Ed.* **2021**, *60*, 10583.
- [18] G. F. Han, F. Li, W. Zou, M. Karamad, J. P. Jeon, S. W. Kim, S. J. Kim, Y. Bu, Z. Fu, Y. Lu, S. Siahrostami, J. B. Baek, *Nat. commun.* **2020**, *11*, 2209.
- [19] H. W. Kim, M. B. Ross, N. Kornienko, L. Zhang, J. Guo, P. Yang, B. D. McCloskey, *Nat. Catal.* **2018**, *1*, 282.
- [20] H. S. Euiyeon Jung, Byoung-Hoon Lee, Vladimir Efremov, Suhyeong Lee, Hyeon Seok Lee, Jiheon Kim, Wytse Hooch Antink, Subin Park, Kug-Seung Lee, Sung-Pyo Cho, Jong Suk Yoo, Yung-Eun Sung, Taeghwan Hyeon *Nat. Mater.* **2020**, *19*, 436.
- [21] Y. Liu, X. Quan, X. Fan, H. Wang, S. Chen, *Angew. Chem. Int. Ed.* **2015**, *54*, 6837.